ORIGINAL ARTICLE

WILEY Cancer Science

Synthetic α-mangostin dilaurate strongly suppresses wide-spectrum organ metastasis in a mouse model of mammary cancer

Masa-Aki Shibata[1] [iD] | Hitomi Hamaoka[1] | Junji Morimoto[2] | Tadashi Kanayama[1] | Kentaro Maemura[1] | Yuko Ito[1] | Munekazu Iinuma[3] | Yoichi Kondo[1]

[1]Department of Anatomy and Cell Biology, Osaka Medical College, Takatsuki, Osaka, Japan

[2]Laboratory Animal Center, Osaka Medical College, Takatsuki, Osaka, Japan

[3]Gifu Pharmaceutical University, Gifu, Japan

Correspondence
Masa-Aki Shibata, Department of Anatomy and Cell Biology, Osaka Medical College, Takatsuki, Osaka, Japan.
Email: an1031@osaka-med.ac.jp

We previously reported that, in a mouse model of mammary cancer, α-mangostin alone exhibits anti-metastatic properties. To enhance this anti-metastatic effect, we examined the efficacy of synthetic α-mangostin dilaurate (MGD), prepared by adding lauric acid to α-mangostin, in the same experimental system wherein mice bearing mammary tumors are exposed to dietary MGD at 0, 2000 and 4000 ppm. Lauric acid has a high propensity for lymphatic absorption, which is the most common pathway of initial dissemination of many solid malignancies. Both mammary tumor volumes and wide-spectrum organ metastasis were markedly reduced at 2000 and 4000 ppm: furthermore, survival in the 4000-ppm group was significantly greater than in control mice. Apoptosis in mammary carcinomas was also significantly increased in the 4000-ppm group, whereas blood microvessel density and lymphatic vessel invasion were markedly reduced. In real-time PCR analyses of tumor samples, increased *p21* and decreased *Pcna* expression were observed with 4000 ppm but values were not statistically significant when compared to expression in control tumors. However, exposure to 4000 ppm significantly decreased expression of phospho-Akt (Ser473/Thr308) as compared to the control, indicating a role in the anti-tumorigenic effects of MGD. These findings suggest that MGD may be useful for adjuvant therapy and chemoprevention and that conjugated medium-chain fatty acids may enhance the efficacy of certain chemotherapeutic agents.

KEYWORDS
α-mangostin, lauric acid, mammary cancer metastasis, mouse, therapeutics

1 | INTRODUCTION

The lethality of breast cancer is due to its high propensity for metastasis to the lymph nodes, lung and bone,[1] thus making more effective and less toxic chemopreventive and anti-metastatic treatments imperative. The pericarp of mangosteen fruit (*Garcinia mangostana* Linn) has a long history of usage as a medicinal plant in South-East Asia.[2] The beneficial actions of mangosteen pericarp extracts have

some scientific support and have gained popularity as natural dietary health supplements. In mammary cancer cells, mangosteen extracts, particularly α-mangostin, induce apoptosis through a mitochondrial pathway and cause cell cycle arrest through induction of p21 and p27 along with Akt dephosphorylation;[3-5] all these effects are mechanistically associated with suppression of in vivo tumor growth and metastasis in mouse mammary cancer models.[4,6] Several other animal models further demonstrate the anti-tumorigenic effects of

mangosteen extracts (eg, inhibition of aberrant crypt foci in rat colon carcinogenesis),[7] and of tumor growth in xenograft animal models of human colorectal[8] and prostate cancers.[9]

Fatty acids are bioactive molecules classified by their carbon atom chain length as short-chain (<8 carbon atoms), medium-chain (8-14 carbon atoms) and long-chain (>16 carbon atoms).[10] While 3-carbon fatty acid chains have been shown to induce apoptosis in several neoplastic cell lines,[11-13] lauric acid, a large component of medium-chain triglycerides, has been reported to inhibit prostate hyperplastic lesions in rats in vivo:[14] in addition, lauric acid has a higher propensity for lymphatic absorption compared to the long-chain octanoic acid,[15,16] which is significant because the most common pathway of initial dissemination of many solid malignancies is known to be via the lymphatics.[17] We wanted, therefore, to determine whether the anti-metastatic properties demonstrated by α-mangostin could be enhanced by the addition of medium-chain lauric acid (C12; dodecanoic acid) to form α-mangostin dilaurate (MGD) in our previously used mouse model of mammary cancer.

2 | MATERIALS AND METHODS

2.1 | α-mangostin dilaurate preparation

We extracted α-mangostin (Figure 1A) from dried mangosteen pericarps and then dissolved 0.01 mol/L α-mangostin in pyridine and tetrahydrofuran before mixing the solution with lauroyl chloride. This solution was heated and cooled, added to 1 N HCl, and extracted with ethyl acetate. Extracts were concentrated and purified by silica gel column chromatography and MGD was collected as a solid pale-yellow substance. The chemical structure of MGD is shown in Figure 1B.

2.2 | Cell line and animals

Mammary tumors arising from BJMC3879 cell implantation have mutant p53 and an especially high metastatic predilection for the lymph nodes and lungs,[18-20] a trait retained through culture. To monitor the in vivo progression and dissemination, we performed a stable transfection of the BJMC3879 parent cell line with *luc2*, an improved *firefly luciferase* gene, to generate the BJMC3879Luc2 mammary carcinoma cell line.[21] BJMC3879Luc2 cells used in this study were maintained in DMEM with 10% FBS and penicillin-streptomycin and grown in an incubator under 5% CO_2 at 37°C.

Forty 5-week-old female BALB/c mice were purchased from Japan SLC, Hamamatsu, Japan. The animals were housed 5 to plastic cage on wood chip bedding with free access to water and food under controlled temperature (21 ± 2°C), humidity (50% ± 10%) and lighting (12-12 hours light-dark cycle). All animal experiments were approved by the Institutional Review Board of the Osaka Medical College (approval no. 20023) and were performed in accordance with the procedures outlined in the Guide for the Animal Care and Use of Laboratory Animals of Osaka Medical College.

2.3 | Experimental design

At 6 weeks of age, we subcutaneously inoculated 40 mice with 2.5×10^6 BJMC3879Luc2 cells in 0.3 mL PBS in the right inguinal region. Two weeks later, we selected 30 mice with mammary tumors approximately 0.3-0.4 cm in diameter; these selected mice were randomly distributed to 3 treatment groups of 10 mice each receiving dietary exposure to MGD at either 0, 2000 or 4000 ppm for an additional 7 experimental weeks. Food and water consumption and individual body weights were recorded weekly, along with measurement of each mammary tumor using digital calipers. Tumor volumes were then recorded based on the formula of maximum diameter × (minimum diameter)^2 × 0.4.[22] The calculated MGD intake (mg/kg body weight/d) was based on food consumption, dietary MGD concentrations and body weight. One hour prior to sacrifice at experimental week 7, all surviving animals were injected intraperitoneally with 50 mg/kg BrdU (Sigma, St. Lois, MO, USA) for immunohistochemical analysis of tumor DNA synthesis. All mice were killed by exsanguination under isoflurane anesthesia.
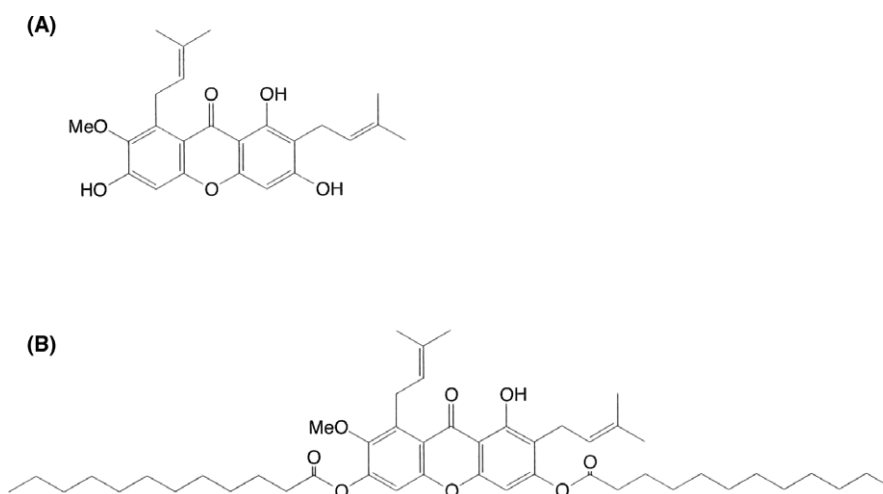

FIGURE 1 The chemical structures of (A) α-mangostin [$C_{24}H_{26}O_6$; molecular weight: 410] and (B) synthetic α-mangostin dilaurate (MGD) [$C_{47}H_{70}O_8$; molecular weight: 762]. The pericarp of the mangosteen contains a class of compounds called xanthones, which include α-mangostin. MGD is prepared by conjugation of lauric acid, a medium-chain fatty acid [C_{12}] to α-mangostin

2.4 | In vivo bioluminescence imaging

At experimental week 6, 5 mice from each group were anesthetized by isoflurane inhalation using an anesthesia system. Each anesthetized mouse received an intraperitoneal injection of 3 mg D-luciferin potassium salt (Wako Pure Chemical Industries, Osaka, Japan) in PBS prior to bioluminescence imaging using a Photon Imager (Biospace Lab, Paris, France).

2.5 | Preparation for histopathological analyses

At necropsy, we harvested tumors and lymph nodes from all mice from the axillary and femoral regions, along with any other lymph nodes that appeared abnormal, and fixed the tissues in 10% phosphate buffered formalin (PBF) solution. Lungs, kidneys, adrenals, ovaries, and other tissues/organs that appeared abnormal were also routinely excised and immersed in PBF for formalin-fixed paraffin-embedded (FFPE) tissues. All FFPE tissues were cut at sequential 4-μm sections for histopathological analysis using H&E and immunohistochemical staining.

2.6 | Immunohistochemistry of mammary carcinomas

We used a Tris-EDTA buffer (pH 9.0) antigen retrieval method (for 10 minutes at 110°C) for all immunohistochemical staining. The primary antibodies used were as follows: anti-p53 mouse monoclonal antibody (Santa Cruz Biotechnology, Santa Cruz, CA, USA), anti-active caspase-3 rabbit polyclonal antibody (Cell Signaling Technology, Danvers, MA, USA), anti-podoplanin hamster monoclonal antibody (AngioBio, Del Mar, CA, USA) and anti-CD31 rabbit polyclonal antibody (Lab Vision, Fremont, CA, USA). We incubated the slides with corresponding biotinylated secondary antibodies using an established labeled streptavidin-biotin method (Dako, Glostrup, Denmark), with exposure to diaminobenzidine and hematoxylin counterstain for visualizing the immunocomplexes formed. In addition, anti-phospho-Akt-Ser473/Thr308 rabbit polyclonal antibody (Cell Signaling Technology) and anti-rabbit Alexa-594 antibody (Thermo Fisher Scientific, Waltham, MA, USA) were used for immunofluorescence staining. Nuclear staining was conducted with DAPI (Vector Labs, Burlingame, CA, USA); phospho-Akt-positive areas and viable regions with DAPI-positive nuclei in the same field were digitally captured at 40× magnification. These digitized images were measured using the ImageJ program (NIHR public domain) and the results are expressed as a percentage of phospho-Akt-positive areas to nuclear-positive areas.

2.7 | Tumor apoptosis and cell proliferation

We examined FFPE tumor sections for quantitative analyses of apoptotic cell death using TUNEL staining (Wako Pure Chemical Industries). TUNEL-positive cells were counted only in viable tumor regions peripheral to the areas of central necrosis. The slides were initially scanned at low-power (×100) magnification to identify areas with the highest number of TUNEL-positive cells. Four areas neighboring a focus of high TUNEL-positivity were selected and counted at higher (×200-400) magnification. The numbers of TUNEL-positive cells were expressed as numbers per cm^2.

For evaluating BrdU labeling indices in tumors, DNA was denatured in situ by incubating unstained FFPE tumor sections in 4 N HCl solution for 20 minutes at 37°C. The numbers of BrdU-positive (S-phase) cells were counted in 4 random high power (×400) fields of viable tissue under a microscope equipped with a digital camera; BrdU labeling indices were expressed as numbers per cm^2.

2.8 | Densities of blood microvessels and lymphatic vessel invasion in tumors

CD31 is a marker for the endothelium of blood vessels, whereas podoplanin is a marker for lymphatic endothelium. Tumor sections were exposed to antibodies for each marker and the numbers of CD31-positive blood microvessels were counted as previously described;[23] briefly, the slides were scanned at low-power (×100) magnification to identify areas with the highest number of CD-31-positive vessels and 5 areas of highest microvascular density were selected for quantitation under higher (×200-400) magnifications. To determine the number of lymphatic vessel invasion in tumors, we counted the number of podoplanin-positive lymphatic vessels containing intraluminal tumor cells in whole tumor sections and expressed as numbers per cm^2.

2.9 | Real-time PCR analysis in tumors

To avoid the inclusion of necrotic and mesenchymal tissues in real-time PCR analysis of Pcna and p21, we specifically microdissected only viable mammary carcinoma tissues from FFPE tumors using a laser microdissector (LMD7000; Leica Microsystems, Wetzlar, Germany). Total RNA was then extracted from microdissected samples using the RNeasy FFPE Kit (Qiagen, GmbH, Hilden, Germany) and cDNA synthesized using a Primer Script RT Reagent Kit with gDNA Eraser (Takara Bio, Otsu, Shiga, Japan). We subsequently amplified resulting cDNA using a Thermal Cycler Dice Real-time System (Takara Bio) and SYBR Premix Ex TaqII (Takara Bio). The Gapdh gene was used as an internal control. Amplification cycles were as follows: an initial step at 95°C for 30 seconds, followed by 45 cycles of 5 seconds at 95°C, 10 seconds at 58°C, and 20 seconds at 72°C. The primer sequences were designed to generate PCR products smaller than 100 bp in FFPE samples and are shown in Table 1. Relative gene expression levels were normalized to Gapdh (ΔCt) and expressed as fold changes calculated using the $2^{-\Delta\Delta Ct}$ method, as described previously.[24]

2.10 | Statistical analysis

Kaplan-Meier survival curves were plotted according to the number of deaths in each group, and the differences in survival rates determined using the log-rank test. The Kruskal-Wallis H-test was conducted; when the data were significant, Dunn's test (a non-parametric multiple comparison) was also used. The Mann-Whitney U-test (an unpaired group and non-parametric analysis) was used to

TABLE 1 Mouse primer sequences for real-time PCR for formalin-fixed paraffin-embedded samples

Genes	Primer sequences (5'->3')		PCR products (bp)
p21	Forward	AACATCTCAGGGCCGAAAAC	60
	Reverse	CGCTTGGAGTGATAGAAATCTGTC	
Pcna	Forward	ACTTGGAATCCCAGAACAGG	55
	Reverse	TTCACCCGACGGCATCT	
Gapdh	Forward	GGAGTAAGAAACCCTGGACCAC	66
	Reverse	AGTTGGGATAGGGCCTCTCTTG	

compare the data generated by real-time PCR analysis in control and 4000 ppm-treated groups. Data are expressed as mean ± SD and differences are considered statistically significant when P < .05.

3 | RESULTS

3.1 | Food/water consumption, survival and body weights

Food consumption values were similar among groups (3.7-4.1 g/mouse/d), but water consumption values showed slight dose-related increases in MGD-treated groups (7.7-9.4 g/mouse/d). Average MGD intake was 359 mg/kg body weight/d in the 2000-ppm group and 753 mg/kg body weight/d in the 4000-ppm group. As shown in the survival rates in Figure 2A, 50% (5 animals) of the control 0-ppm group died by week 7 (experimental day 48) due to widespread metastasis of mammary carcinoma (1 case was excluded from further analysis because of organ loss due to cannibalism), while only 10% (1 mouse) from the 2000-ppm group succumbed by week 7. There were no deaths in the 4000-ppm group. The body weight changes in control and MGD-treated mice are shown in Figure 2B. Statistically, the body weights of control and MGD-treated mice did not differ throughout the duration of the experiment.

3.2 | Tumor growth and bioluminescence imaging

Except in experimental week 5, tumor volumes were significantly inhibited in both MGD-treated groups throughout the duration of the experiment (Figure 2C); the MGD tumor volumes showed the same downward trend at week 5 but were not statistically significant. Bioluminescence imaging revealed metastatic signals in the mandibular, axillary and inguinal regions of mice from all groups, but there was a decrease in metastatic expansion in MGD-treated mice compared to that in control animals (Figure 2D).
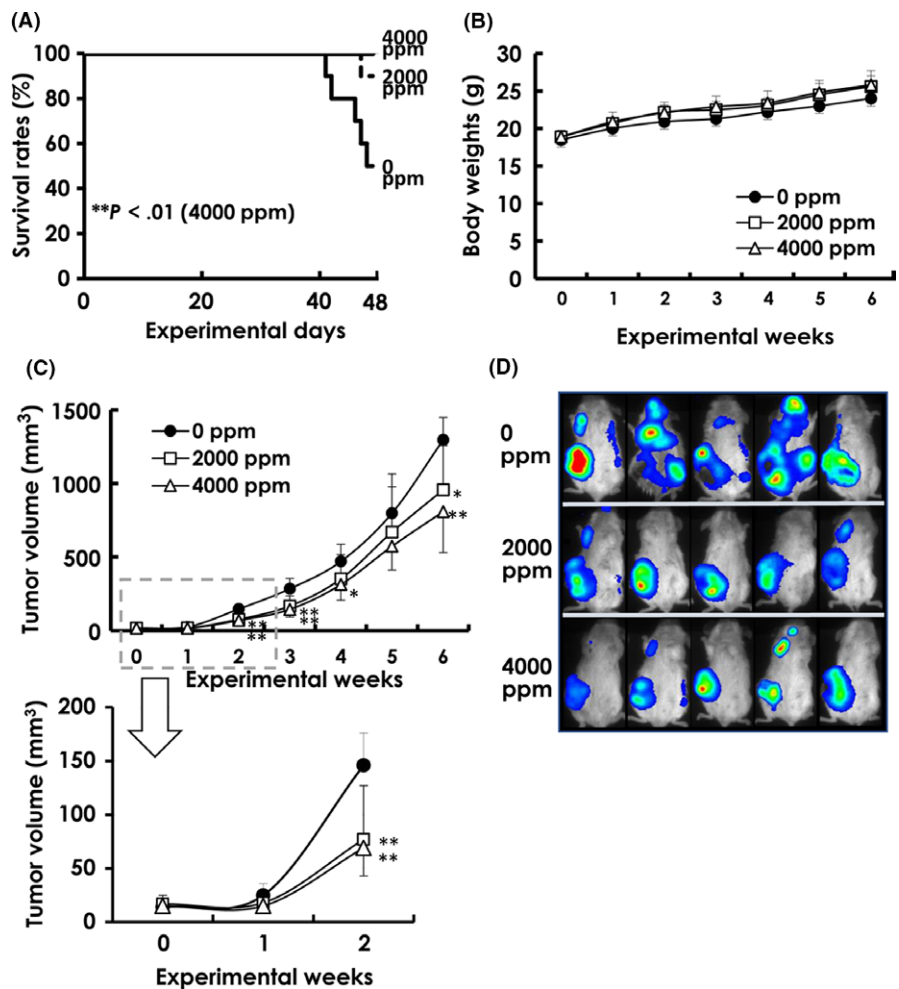

FIGURE 2 (A) Survival rates in the 4000-ppm group were significantly higher than in the control group, whereas body weights (B) of mice given α-mangostin dilaurate (MGD) were comparable to those in the control group. C, Tumor volumes were smaller with continuous exposure to both 2000 and 4000 ppm. D, Bioluminescence imaging in 5 representative mice from each group. Bioluminescence imaging demonstrated decreases in the extension of metastasis in MGD-treated groups compared to the control group. *P < .05, **P < .01

3.3 | Metastasis of mammary carcinomas

Primary mammary carcinomas induced by BJMC3879Luc2 inoculation proved to be mutant p53 protein-positive adenocarcinomas showing less glandular formation (Figure 3A)[25] (Figure 3B). Representative lymph node metastases are shown in Figure 3C,D. The number of metastasis-positive lymph nodes per mouse was significantly decreased in both the 2000-ppm and 4000-ppm groups compared to that in the control group (Figure 3G). Metastatic lung foci were larger and more frequent in control mice (Figure 3E) compared to those in MGD-treated mice (Figure 3F), and the number of metastatic foci ≥250 μm was also significantly decreased in both MGD-treated groups (Figure 3H). Metastatic foci were also observed in the kidneys, adrenals, ovaries and mediastinum (Figure 4A-D).
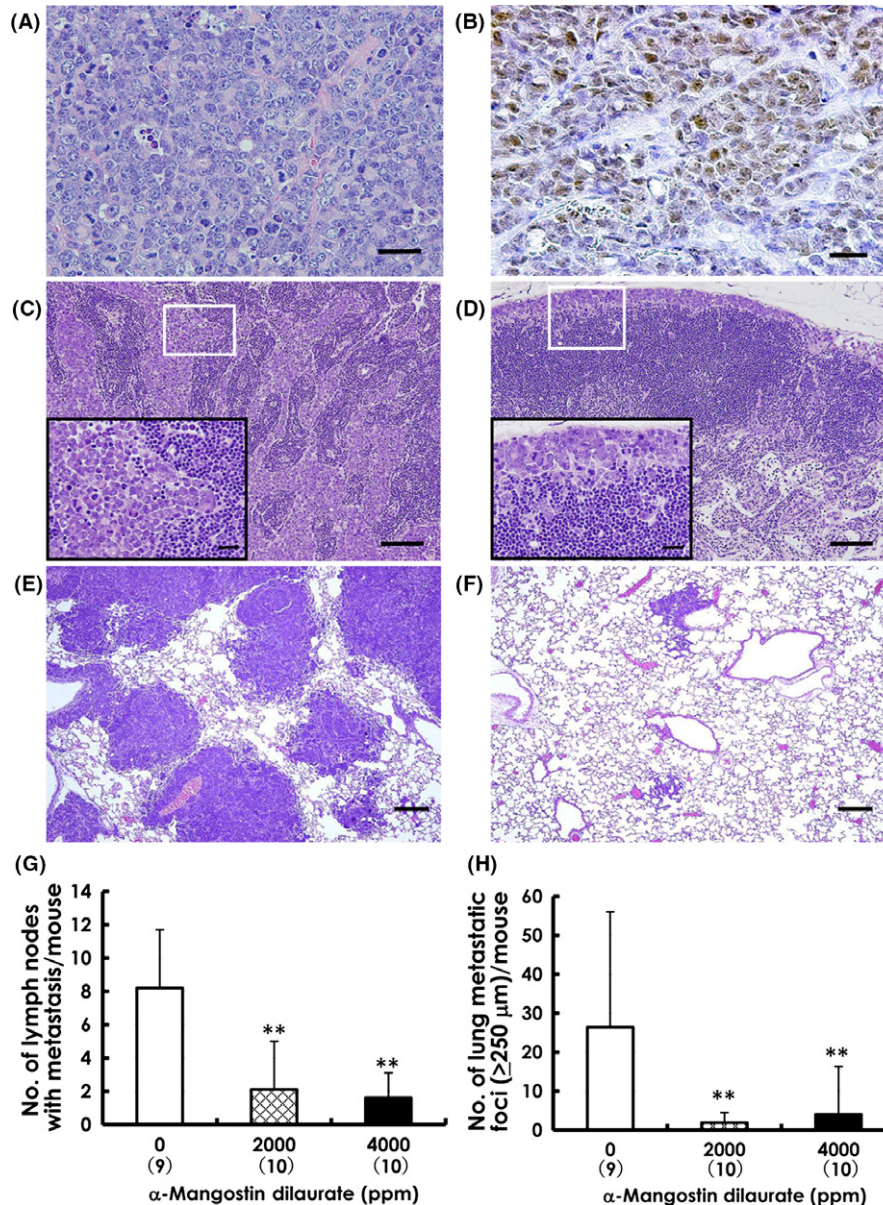

FIGURE 3 A, Mammary carcinomas induced by BJMC3879Luc2 cells proved to be adenocarcinomas with infrequent glandular formation. Many mitotic and some apoptotic cells were seen. B, p53 immunohistochemistry on a mammary carcinoma sample. Note the nuclear staining indicative of mutant p53 protein. C, Metastasis to a lymph node in a control mouse. Metastatic carcinoma cells filled the sinusoidal space (inset: higher magnification of the white-edged rectangular area). D, A lymph node from a mouse administered 4000-ppm α-mangostin dilaurate (MGD). Metastatic carcinoma cells filled the subcapsular sinus (inset: higher magnification of white-edged area). E, Metastatic foci in the lung of a control mouse. Many metastatic foci and small to large nodules were seen. F, Metastatic foci in the lungs of a mouse administered 4000-ppm MGD; metastatic foci were fewer and much smaller. G, Multiplicity of lymph node metastasis was significantly decreased in both MGD-treated groups. H, Multiplicity of lung metastatic foci measuring ≥250 μm was significantly reduced in both MGD-treated groups. A and C-F, H&E. B, p53 immunohistochemistry. Scale bars: (A,B) 20 μm; (C,D) 100 μm (insets, 50 μm); (E,F) 200 μm; **$P < .01$; numerals in parentheses indicate the number of animals examined
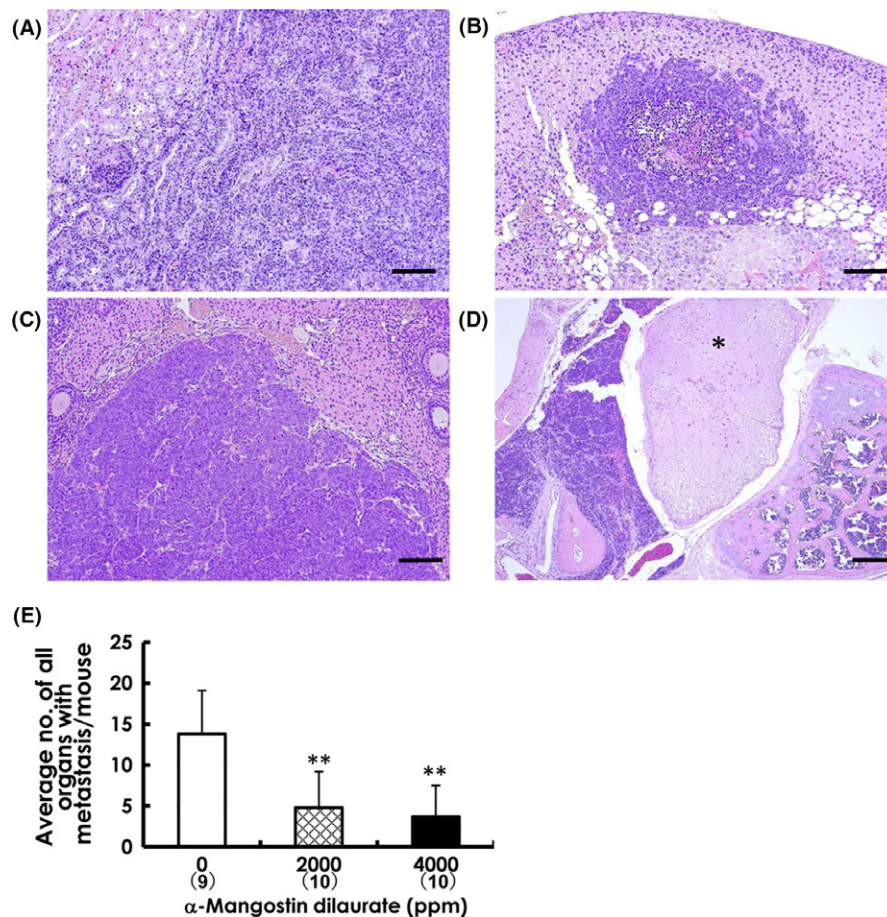
FIGURE 4 Mammary carcinoma metastases in other organs. A, Renal metastasis in a control mouse. B, Metastasis to the adrenal of a control mouse. C, Ovarian metastasis in a mouse given 4000-ppm α-mangostin dilaurate (MGD). D, Metastasis to the mediastinum of a control mouse; * indicates spinal cord. E, The average number of all organs with metastases per mouse was significantly reduced at both 2000-ppm and 4000-ppm groups. (A-D) H&E stain; scale bars: (A-C) 100 μm, (D) 200 μm; **P < .01; numerals in parentheses indicate the number of animals examined

When evaluating the relative number of affected organs, unilateral metastasis in bilateral organs like kidneys was counted as 1 case, and bilateral metastases were counted as 2 cases. The average number of all organs with metastasis per mouse was distinctly lower in both MGD-treated groups compared with the control group (Figure 4E).

3.4 | Apoptosis and cell proliferation in mammary carcinomas

Representative tumor sections showing TUNEL-positive apoptotic cells are presented in Figure 5A,B. Results of quantitative analyses for apoptosis in mammary tumors are shown in Figure 5E. The number of TUNEL-positive cells was significantly increased in tumors exposed to 4000-ppm MGD compared to the tumors from control mice (Figure 5E). In addition, the expression of active caspase-3 was much higher in mammary tumors treated with MGD (inset, Figure 5B) than in the control tumors (inset, Figure 5A), suggesting that MGD administration induced apoptotic cell death. Increased caspase-3 activity in vivo is notable because caspase-3 is the final

executor of apoptosis and the most significant member of the apoptotic pathway.

Cell proliferation was examined in the mammary carcinomas of MGD-treated mice using BrdU immunohistochemistry, as shown in Figure 5C,D. The BrdU labeling indices in tumors were decreased in both MGD-treated groups in a dose-dependent manner, but not to a statistically significant level (Figure 5F).

3.5 | Blood microvascular densities and lymphatic vessel invasion

Blood microvascular density determined by CD31 immunohistochemistry (arrows in Figure 6A,B) was significantly decreased in the 4000-ppm group compared to that in the control group (Figure 6E). Tumor cells found within the lumina of dilated podoplanin-positive lymphatic vessels of tumors in both the control (Figure 6C) and MGD-treated animals (Figure 6D) indicated the occurrence of lymphatic vessel invasion; however, the numbers of invaded lymphatic vessels decreased in mammary tumors from both MGD-treated groups (Figure 6F), but statistical significance was observed only at
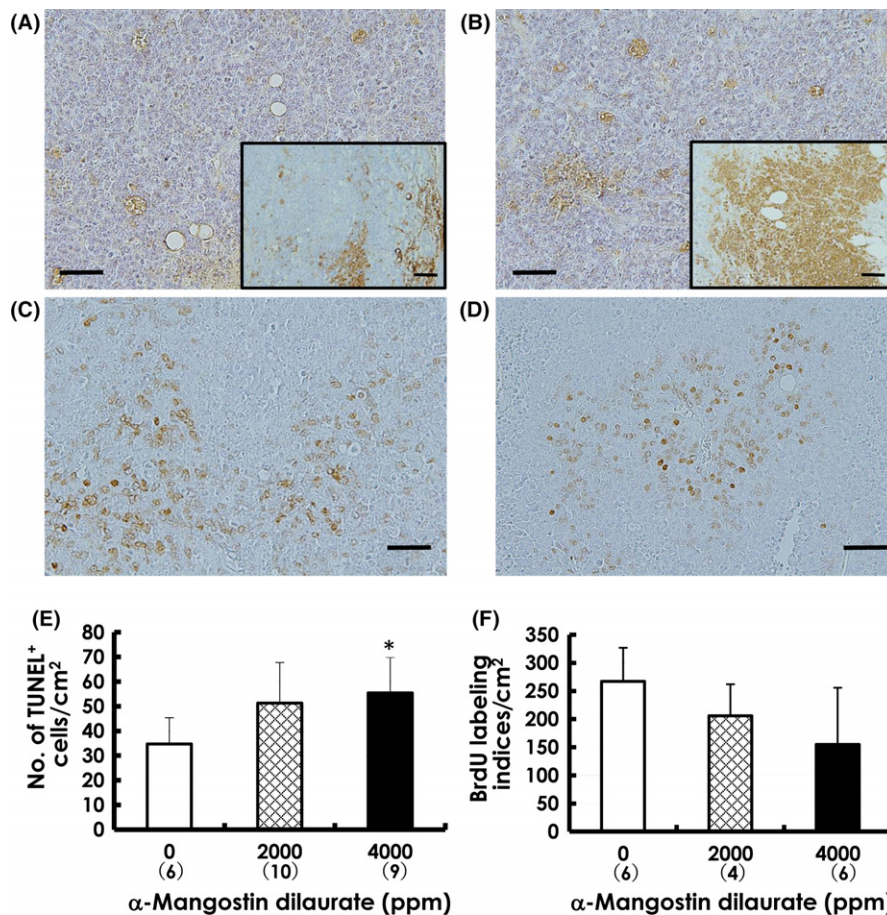
FIGURE 5 Apoptosis and cell proliferation in mammary carcinomas. The number of TUNEL-positive apoptotic cells (A,B) was much higher in the tumor of a mouse administered 4000-ppm α-mangostin dilaurate (MGD) (B) than in the tumor of a control mouse (A). Expression of active caspase-3 was more pronounced in the tumor of a mouse on 4000-ppm MGD (inset B) than in a control mouse (inset A). The number of TUNEL-positive cells was significantly increased in the 4000-ppm group compared to the control group (E). The numbers of BrdU-labeled cells tended to be lower in the 4000-ppm group (D) than in the 0-ppm group (C), but the values were not statistically significant (F). A, B TUNEL reaction; (inset A, inset B) active caspase-3 immunohistochemistry; (C,D) BrdU immunohistochemistry. Scale bars: 50 μm; *$P < .05$; numerals in parentheses indicate the number of animals examined

2000-ppm MGD, indicating a reduction in potential metastatic migration via the lymphatic vessels of treated tumors.

3.6 | Transcriptional levels of *p21* and *Pcna* in mammary carcinomas

Samples from FFPE mammary carcinomas, microdissected from surrounding mesenchyma (Figure 7A) and necrosis, provided viable and pure tumor tissues for evaluating the expression of *p21* and *Pcna* by real-time PCR. Compared to tissues from control mice, *p21* showed a 25% increase in tissues from mice treated with 4000 ppm, whereas *Pcna* levels decreased by 23% (Figure 7B). However, these fluctuations were not statistically significant.

3.7 | Effects of Akt phosphorylation by α-mangostin dilaurate

Although phospho-Akt expression was observed in mammary carcinomas from both the control and 4000-ppm MGD groups, the control tumors (Figure 8A,C) showed a tendency toward more phospho-Akt-positive areas than did tumors exposed to 4000-ppm MGD (Figure 8D,F). As shown in Figure 8G, the percentage of phospho-Akt-positive areas (Figure 8A,D) to that of DAPI-positive areas (Figure 8B,E) was significantly less in the 4000-ppm group compared with those in the control group.

4 | DISCUSSION

Tumors induced with BJMC3879Luc2 mammary cancer cells have mutant p53 protein that confers a high propensity for metastasis to the lymph nodes and lungs,[4,20,26] similar to the etiology seen in human breast cancers.[1] Using this murine model of mammary carcinoma, we previously reported that both pure α-mangostin and panaxanthone (comprising 75%-85% α-mangostin and 5%-15% γ-mangostin) suppress metastasis to the lymph nodes and lungs through induction of apoptosis via a mitochondrial pathway, G1 arrest in the cell cycle by induction of p21 and p27, PCNA inhibition
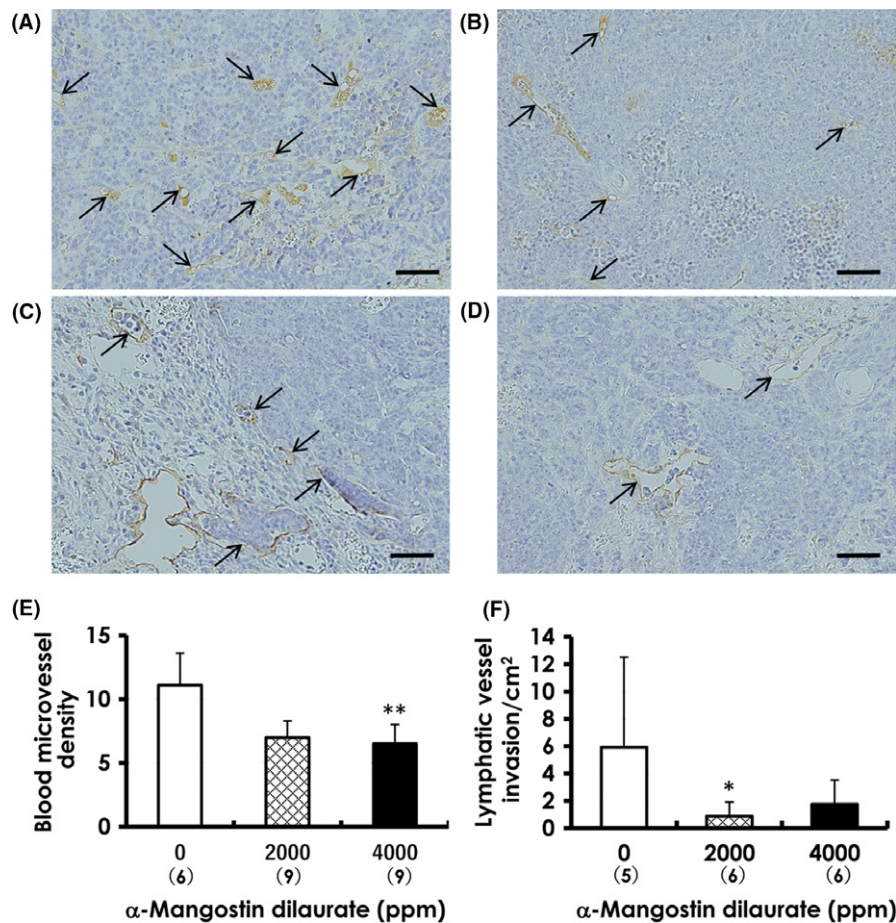
FIGURE 6 Angiogenesis and lymphatic vessel invasion in mammary carcinomas. The numbers of CD31-positive blood microvessels (arrows, A,B) tended to be lower in the α-mangostin dilaurate (MGD)-treated groups (B) as compared to the control group (A). CD31-positive blood microvessel density in tumors was significantly decreased with exposure to 4000-ppm MGD (E). Podoplanin-positive lymphatic vessels of tumors were often dilated and filled with tumor cells (arrows, C,D), indicative of lymphatic vessel invasion. The frequency of lymphatic vessel invasion in tumors from MGD-treated mice (D) was decreased compared to that in control mice (C). Number of lymphatic vessel invasion per cm^2 tumor was much lower in MGD-treated mice than in the control group, but was statistically significant only at 2000 ppm (F). (A,B) CD31 immunohistochemistry; (C,D) podoplanin immunohistochemistry. Scale bars: 50 μm; *$P < .05$; **$P < .01$; numerals in parentheses indicate the number of animals examined

and certain anti-angiogenesis effects.[3-6] PCNA is essential for replication[27] and p21 has been shown to interact with PCNA and induce arrest at G1.[28,29] Increased *p21* and decreased *Pcna* mRNA levels were observed in the 4000-ppm tissues with real-time PCR analysis. Because cancer is characterized by uncontrolled cell proliferation resulting from abnormal activity of various cell cycle proteins, cell cycle regulators are considered attractive targets in cancer therapy.[30]

Fatty acids are bioactive molecules classified as short-chain, medium-chain and long-chain in terms of the number of carbon atoms present in the chain. On their own, fatty acids are known to induce apoptosis in cancer cell lines,[12,13] and the number of carbon atoms (C*n*) in their chains are believed to be a critical factor influencing their cytotoxicity.[11] Compared to short-chain fatty acids like butyrate, the medium-chain lauric acid induces preferential apoptosis and is associated with suppression of cell cycle processes as well as increased generation of glutathione-independent reactive oxygen

species.[31] Oral administration of either lauric acid (C12) or myristic acid (C14) significantly inhibits in vivo development of testosterone-induced prostatic hyperplasia in rats[14] and evidence for the anti-proliferative effects, particularly of lauric acid, is accumulating. Although there is some overlap in the cumulative absorption of medium-chain and long-chain fatty acids via the portal vein and lymphatics, there are significant differences in their routes and rates of absorption. For example, approximately 4 times as much as lauric acid is absorbed via the lymphatics vs the portal vein, whereas the opposite is true for long-chain octanoic acid.[15,16] It should be noted that the most common pathway of initial dissemination of various solid malignancies is the lymphatic system.[17] Lauric acid is further reported to possess anti-viral[32] and anti-bacterial[33] properties and can destroy lipid-coated viruses. Breast milk contains high concentrations of both lauric and myristic acids,[34] contributing to the myriad health benefits for breast-fed infants. Medium-chain fatty acids are also less efficiently stored in the body than other fatty acids and are highly prone
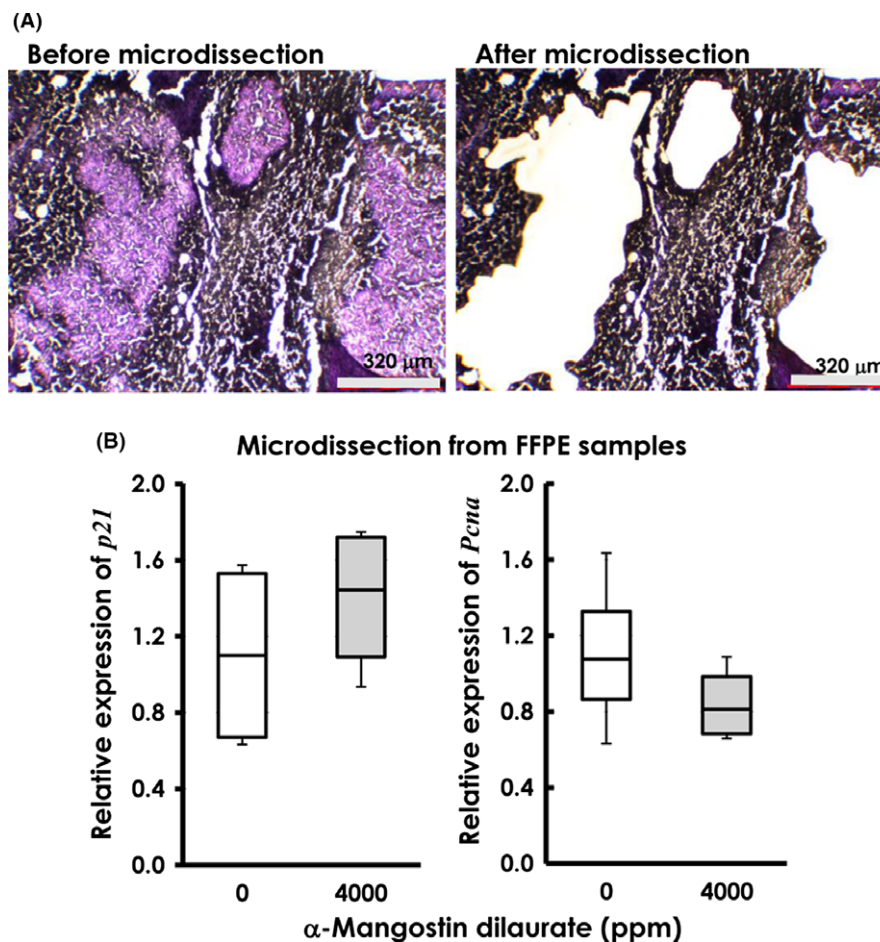
FIGURE 7 A, Viable regions of mammary carcinomas were microdissected from formalin-fixed paraffin-embedded (FFPE) samples to exclude the mesenchymal and necrotic tissues (hematoxylin counterstain); *p21* and *Pcna* levels in microdissected sections were then analyzed by real-time PCR. B, Box and whisker plot showing the relative expression levels for *p21* and *Pcna* in FFPE tumor samples. An increase in the relative levels of *p21* and a decrease in relative levels of *Pcna* were observed in tissues from the 4000-ppm group, but neither was statistically significant. The boxes represent the 25th to 75th percentiles, and horizontal lines within the box represent median values. The whiskers extend either to 10th and 90th percentiles, respectively. The number of mice examined was reduced to 4 in each group due to degraded RNA from FFPE samples causing poor amplification and/or aberrant dissociation temperatures of *Gapdh*

to oxidative metabolism once ingested, implying that they are unlikely to contribute to obesity via direct storage in adipocytes, and may be useful in dietary regimens.[35]

In this study, synthetic MGD significantly suppressed wide-spectrum organ metastasis, including that to the lymph nodes and lungs. We were unable to include an α-mangostin-treated group in this study because of the high cost of purified α-mangostin and could not, therefore, directly compare the anti-tumor effects of α-mangostin and MGD. A previous study using α-mangostin at the same dietary concentration (4000 ppm)[36] revealed a 2-fold amplification of inhibitory effects by MGD on lung and lymph node metastasis compared with mice given α-mangostin alone (42% vs 23%).

Neovascularization through angiogenesis is a key process in the growth of solid tumors, both primary and metastatic; tumors do not grow beyond a few cubic millimeters unless a vascular network is established to feed further expansion.[37] This makes inhibition of angiogenesis and hematogenous metastases crucial targets of cancer therapies.[38] However, as previously stated, the lymphatic system is

the most common pathway of initial spread of solid tumors[17] and, thus, constitutes another front for the treatment and inhibition of metastatic spread. In fact, lymph node metastasis is the most clinically influential prognostic factor in cases of breast cancer.[39] MGD significantly inhibited the multiplicity of lymph node metastasis in mice administered either dose in the current study, supported by a significant reduction in the frequency of lymphatic vessel invasion in the MGD-treated mice.

Akt phosphorylation contributes to cell proliferation, apoptotic cell death, cell cycle entry, angiogenesis and metastasis: all important aspects of the oncogenic process.[40] To be fully activated, Akt requires phosphorylation at 2 specific amino acid residues, Thr308 and Ser473. Several modes of Akt dysregulation have been identified in various types of cancer, including breast cancer, which ultimately affect such processes as cell growth, survival, proliferation, motility and/or invasion.[40] The present study demonstrated that MGD administration decreased expression of phospho-Akt (Ser473/Thr308). The inhibition of tumor growth, angiogenesis and
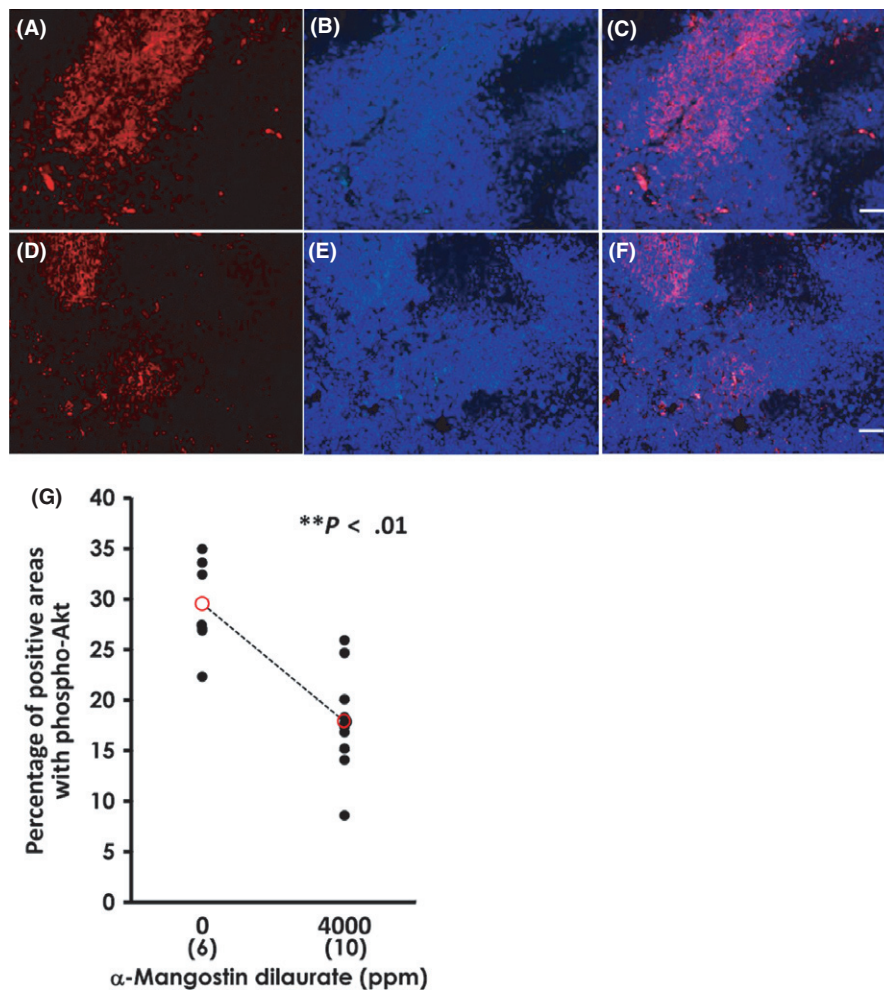
FIGURE 8 Immunofluorescence staining with phospho-Akt (red-Alexa-594). Merging images (C,F) with phospho-Akt (A,D) and DAPI (D,E) showed a tendency for far less expansion of phospho-Akt-positive areas in a mouse receiving 4000-ppm compared to tissue from a control. As presented in a scatter plot diagram (G, red circle indicates mean), the percentage of areas demonstrating phospho-Akt expression was significantly decreased in the 4000-ppm MGD group compared to that in the control group. Scale bars: 50 μm; [G] **P < .01; numerals in parentheses indicate the number of animals examined

metastasis in conjunction with increased apoptosis and alterations in cell-cycle molecules that we observed may be at least partially due to decreased Akt-phosphorylation. In addition, although the p53/Akt network is an important module that controls pathways to cell survival or death,[41] because the mammary carcinoma cells used in the present study contain mutant p53, Akt regulation observed in the present study was considered to be p53-independent. Akt inhibitors have shown significant promise preclinically and are now in clinical trials;[42] in fact, the PI3K/Akt pathway is now considered to be an important therapeutic target in cancer treatment.

Dietary administration of MGD strongly suppressed tumor growth and metastases to a wide spectrum of organs in BJMC3879Luc2-inoculated mice. Because these cells carry mutant p53, these inhibitory effects likely occur through a p53-independent mechanism involving suppression of Akt phospohorylation. Approximately half of human cancers harbor *p53* mutations[43] and, thus, MGD may be highly relevant to human cancer therapy. This study also indicates the benefit of conjugation with medium-chain

fatty acids to enhance the effects of certain chemotherapeutic agents.

CONFLICT OF INTEREST

The authors have no conflicts of interest to declare.

ORCID

Masa-Aki Shibata http://orcid.org/0000-0002-3350-7305

REFERENCES

1. Nguyen DX, Massague J. Genetic determinants of cancer metastasis. *Nat Rev Genet*. 2007;8:341-352.

2. Wexler B. *Mangosteen*. Salt Lake City, UT: Woodland Publishing; 2007.

3. Akao Y, Nakagawa Y, Iinuma M, Nozawa Y. Anti-cancer effects of xanthones from pericarps of mangosteen. *Int J Mol Sci*. 2008;9:355-370.

4. Shibata MA, Iinuma M, Morimoto J, et al. α-Mangostin extracted from the pericarp of the mangosteen (*Garcinia mangostana* L.) reduces tumor growth and lymph node metastasis in an immunocompetent xenograft model of metastatic mammary cancer carrying a p53 mutation. *BMC Med*. 2011;9:69.

5. Kurose H, Shibata MA, Iinuma M, Otsuki Y. Alterations in cell cycle and induction of apoptotic cell death in breast cancer cells treated with α-mangostin extracted from mangosteen pericarp. *J Biomed Biotechnol*. 2012;2012:672428.

6. Doi H, Shibata MA, Shibata E, et al. Panaxanthone isolated from pericarp of *Garcinia mangostana* L. suppresses tumor growth and metastasis of a mouse model of mammary cancer. *Anticancer Res*. 2009;29:2485-2495.

7. Nabandith V, Suzui M, Morioka T, et al. Inhibitory effects of crude α-mangostin, a xanthone derivative, on two different categories of colon preneoplastic lesions induced by 1, 2-dimethylhydrazine in the rat. *Asian Pac J Cancer Prev*. 2004;5:433-438.

8. Aisha AF, Abu-Salah KM, Ismail Z, Majid AM. In vitro and in vivo anti-colon cancer effects of *Garcinia mangostana* xanthones extract. *BMC Complement Altern Med*. 2012;12:104.

9. Johnson JJ, Petiwala SM, Syed DN, et al. α-Mangostin, a xanthone from mangosteen fruit, promotes cell cycle arrest in prostate cancer and decreases xenograft tumor growth. *Carcinogenesis*. 2012;33:413-419.

10. Beermann C, Jelinek J, Reinecker T, Hauenschild A, Boehm G, Klor HU. Short term effects of dietary medium-chain fatty acids and n-3 long-chain polyunsaturated fatty acids on the fat metabolism of healthy volunteers. *Lipids Health Dis*. 2003;2:10.

11. Lima TM, Kanunfre CC, Pompeia C, Verlengia R, Curi R. Ranking the toxicity of fatty acids on Jurkat and Raji cells by flow cytometric analysis. *Toxicol In Vitro*. 2002;16:741-747.

12. Fauser JK, Prisciandaro LD, Cummins AG, Howarth GS. Fatty acids as potential adjunctive colorectal chemotherapeutic agents. *Cancer Biol Ther*. 2011;11:724-731.

13. Matthews GM, Howarth GS, Butler RN. Short-chain fatty acids induce apoptosis in colon cancer cells associated with changes to intracellular redox state and glucose metabolism. *Chemother*. 2012;58:102-109.

14. Veeresh Babu SV, Veeresh B, Patil AA, Warke YB. Lauric acid and myristic acid prevent testosterone induced prostatic hyperplasia in rats. *Eur J Pharmacol*. 2010;626:262-265.

15. Sigalet DL, Winkelaar GB, Smith LJ. Determination of the route of medium-chain and long-chain fatty acid absorption by direct measurement in the rat. *JPEN*. 1997;21:275-278.

16. Sigalet DL, Martin G. Lymphatic absorption of glucose and fatty acids as determined by direct measurement. *J Pediatr Surg*. 1999;34:39-43.

17. Sleeman JP. The lymph node as a bridgehead in the metastatic dissemination of tumors. *Recent Results Cancer Res*. 2000;157:55-81.

18. Shibata MA, Morimoto J, Otsuki Y. Suppression of murine mammary carcinoma growth and metastasis by HSV*tk*/GCV gene therapy using *in vivo* electroporation. *Cancer Gene Ther*. 2002;9:16-27.

19. Shibata MA, Morimoto J, Shibata E, Otsuki Y. Combination therapy with short interfering RNA vectors against VEGF-C and VEGF-A suppresses lymph node and lung metastasis in a mouse immunocompetent mammary cancer model. *Cancer Gene Ther*. 2008;15:776-786.

20. Shibata MA, Ambati J, Shibata E, et al. The endogenous soluble VEGF receptor-2 isoform suppresses lymph node metastasis in a mouse immunocompetent mammary cancer model. *BMC Med*. 2010;8:69.

21. Shibata MA, Shibata E, Morimoto J, et al. An immunocompetent murine model of metastatic mammary cancer accessible to bioluminescence imaging. *Anticancer Res*. 2009;29:4389-4396.

22. Shibata MA, Liu M-L, Knudson MC, et al. Haploid loss of *bax* leads to accelerated mammary tumor development in C3(1)/SV40-TAg transgenic mice: reduction in protective apoptotic response at the preneoplastic stage. *EMBO J*. 1999;18:2692-2701.

23. Gorrin-Rivas MJ, Arii S, Furutani M, et al. Mouse macrophage metalloelastase gene transfer into a murine melanoma suppresses primary tumor growth by halting angiogenesis. *Clin Cancer Res*. 2000;6:1647-1654.

24. Livak KJ, Schmittgen TD. Analysis of relative gene expression data using real-time quantitative PCR and the $2(-\Delta\Delta C(T))$ method. *Methods*. 2001;25:402-408.

25. Shibata MA, Ito Y, Morimoto J, Otsuki Y. Lovastatin inhibits tumor growth and lung metastasis in mouse mammary carcinoma model: a p53-independent mitochondrial-mediated apoptotic mechanism. *Carcinogenesis*. 2004;25:1887-1898.

26. Shibata MA, Shibata E, Morimoto J, Harada-Shiba M. Therapy with siRNA for *Vegf-c* but not for *Vegf-d* suppresses wide-spectrum organ metastasis in an immunocompetent xenograft model of metastatic mammary cancer. *Anticancer Res*. 2013;33:4237-4247.

27. Georgakilas AG, Martin OA, Bonner WM. p21: a two-faced genome guardian. *Trends Mol Med*. 2017;23:310-319.

28. Carnero A. Targeting the cell cycle for cancer therapy. *Br J Cancer*. 2002;87:129-133.

29. Vairapandi M, Azam N, Balliet AG, Hoffman B, Liebermann DA. Characterization of MyD118, Gadd45, and proliferating cell nuclear antigen (PCNA) interacting domains. PCNA impedes MyD118 AND Gadd45-mediated negative growth control. *J Biol Chem*. 2000;275:16810-16819.

30. Otto T, Sicinski P. Cell cycle proteins as promising targets in cancer therapy. *Nat Rev Cancer*. 2017;17:93-115.

31. Fauser JK, Matthews GM, Cummins AG, Howarth GS. Induction of apoptosis by the medium-chain length fatty acid lauric acid in colon cancer cells due to induction of oxidative stress. *Chemother*. 2013;59:214-224.

32. Hornung B, Amtmann E, Sauer G. Lauric acid inhibits the maturation of vesicular stomatitis virus. *J Gen Virol*. 1994;75(Pt 2):353-361.

33. Sun CQ, O'Connor CJ, Roberton AM. The antimicrobial properties of milkfat after partial hydrolysis by calf pregastric lipase. *Chem Biol Interac*. 2002;140:185-198.

34. Lubetzky R, Zaidenberg-Israeli G, Mimouni FB, et al. Human milk fatty acids profile changes during prolonged lactation: a cross-sectional study. *IMAJ*. 2012;14:7-10.

35. McCarty MF, DiNicolantonio JJ. Lauric acid-rich medium-chain triglycerides can substitute for other oils in cooking applications and may have limited pathogenicity. *Open Heart*. 2016;3:e000467.

36. Shibata MA, Kusakabe M, Shibata E, et al. Treatment with tenascin C antibody and/or α-mangostin reduces tumor growth and lymph node metastasis in a model of metastatic mammary cancer. *BAOJ Cancer Res Ther*. 2015;1:011.

37. Folkman J. Angiogenesis-dependent diseases. *Semin Oncol*. 2001;28:536-542.

38. Carmeliet P, Jain RK. Angiogenesis in cancer and other diseases. *Nature*. 2000;407:249-257.

39. Tang C, Wang P, Li X, et al. Lymph node status have a prognostic impact in breast cancer patients with distant metastasis. *PLoS ONE*. 2017;12:e0182953.

40. Agarwal A, Das K, Lerner N, et al. The AKT/I kappa B kinase pathway promotes angiogenic/metastatic gene expression in colorectal cancer by activating nuclear factor-kappa B and β-catenin. *Oncogene*. 2005;24:1021-1031.

41. Wee KB, Aguda BD. Akt versus p53 in a network of oncogenes and tumor suppressor genes regulating cell survival and death. *Biophys J*. 2006;91:857-865.

42. Sarker D, Reid AH, Yap TA, de Bono JS. Targeting the PI3K/AKT pathway for the treatment of prostate cancer. *Clin Cancer Res*. 2009;15:4799-4805.

43. Greenblatt MS, Bennett WP, Hollstein M, Harris CC. Mutations in the p53 tumor suppressor gene: clues to cancer etiology and molecular pathogenesis. *Cancer Res*. 1994;54:4855-4878.